RESEARCH PAPER

A pharmacokinetic–pharmacodynamic model predicting tumour growth inhibition after intermittent administration with the mTOR kinase inhibitor AZD8055

Correspondence James W.T. Yates, Oncology IMED, AstraZeneca Pharmaceuticals, Hodgkin Building, Cambridge, CB10 1XL, UK. E-mail: james.yates@astrazeneca.com

James W T Yates[1],* , Sarah V Holt[1],*, Armelle Logie[1],*, Kirsty Payne[1], Karen Woods[1], Robert W Wilkinson[1,2], Barry R Davies[1] and Sylvie M Guichard[1]

[1]AstraZeneca, Cambridge, UK, and [2]Oncology Research, MedImmune Limited, Cambridge, UK

*The first three authors contributed equally to the work presented here.

BACKGROUND AND PURPOSE

AZD8055 is a potent orally available mTOR kinase inhibitor with *in vitro* and *in vivo* antitumour activity against a range of tumour types. Preclinical studies showed that AZD8055 induced a dose-dependent pharmacodynamic effect in xenograft models *in vivo*, but a lack of understanding of the relative contributions of the maximum inhibition of the biomarkers and the duration of inhibition to the antitumour effect, limited the rational design of experiments to optimize the dose and schedules of treatment.

EXPERIMENTAL APPROACH

In this study, a mathematical modelling approach was developed to relate pharmacodynamics and antitumour activity using preclinical data generated in mice bearing U87-MG xenografts.

KEY RESULTS

Refinement and validation of the model was carried out in a panel of additional human tumour xenograft models with different growth rates and different sensitivity to AZD8055 (from partial growth inhibition to regression). Finally, the model was applied to accurately predict the efficacy of high, intermittent dosing schedules of AZD8055.

CONCLUSIONS AND IMPLICATIONS

Overall, this new model linking pharmacokinetics, pharmacodynamic biomarkers and efficacy across several tumour xenografts with different sensitivity to AZD8055 was able to identify the optimal dose and route of administration to maximize the antitumour efficacy in preclinical models and its potential for translation into man.

Abbreviations

PD, pharmacodynamics; PK, pharmacokinetics

Introduction

The **phosphatidylinositol 3-kinase** (PI3K) pathway is a key signalling pathway in cancer. mTOR is a serine/threonine kinase acting as a sensor of mitogen, energy and nutrient levels and a central controller of cell growth downstream of PI3K (Laplante and Sabatini, 2012). Many therapeutic strategies are currently in development to inhibit the PI3K/mTOR signalling pathway (Chiarini *et al.*, 2015). Allosteric inhibitors of **mTOR** such as **rapamycin** have clinical activity but reactivate PI3K signalling due to feedback (O'Reilly *et al.*, 2006). In patients with **PTEN**-negative glioma, this impaired the clinical activity of rapamycin (Cloughesy *et al.*, 2008). **AZD8055** is a potent and selective inhibitor of mTOR kinase (Chresta *et al.*, 2010). mTOR signals in two distinct complexes, mTORC1 and mTORC2. AZD8055 decreases the phosphorylation of downstream effectors of mTORC1, **S6K** (Ser^{389}) and 4E-BP1 (Ser^{65} and Thr$^{37/46}$) and downstream effectors of mTORC2, **Akt** (Ser^{473}) and NDRG1 (Ser^{422}) *in vitro* and *in vivo* (Garcia-Martinez and Alessi, 2008). Chronic administration of AZD8055 induces a broad antitumour effect in xenograft models across different human tumour types, but it is mostly cytostatic (Chresta *et al.*, 2010).

Several pharmacokinetic (PK)/pharmacodynamic (PD) and efficacy models have been developed for allosteric mTOR inhibitors such as **everolimus** or more recently PI3K and PI3K/mTOR kinase inhibitors (Tanaka *et al.*, 2008; Salphati *et al.*, 2010, 2012). For everolimus, a PK/PD relationship between biomarker data obtained from surrogate tissues and antitumour efficacy suggested that human drug exposure was comparable with that observed in preclinical models at efficacious doses (Tanaka *et al.*, 2008). More recently, a PK/PD model using biomarker modulation in tumours with a pan-PI3K inhibitor **GDC-0941** established a threshold of chronic biomarker modulation to drive tumour stasis (Salphati *et al.*, 2010). A similar study with the mixed PI3K/mTOR inhibitor **GDC-0980** proposed a predicted dose for human efficacy by substituting the preclinical PK parameters for the human PK parameters (Salphati *et al.*, 2012). None of these reports models the relationship between PK, PD and efficacy across a range of xenografted tumour models.

Dose and schedule can significantly affect the antitumour effect of targeted agents, and Solit *et al.* (2005) previously demonstrated that pulsatile dosing at high doses with **gefitinib** could modulate the biological mechanism of action from growth inhibition to cell death in models unresponsive to gefitinib. Phase 1 studies with agents targeting the PI3K and mTOR pathways have tested different dose and schedules to mitigate some of the adverse events associated with these agents. However, there is limited information on the rational alteration of dose and schedules based on PK/PD/efficacy modelling.

The current study reports the development of a PK/PD model with AZD8055 across a number of preclinical models with differential antitumour effects. This mathematical modelling approach tests the hypothesis that there is a quantitative relationship between drug exposure, using plasma as a surrogate for tissue exposure, the observed response on pathway biomarkers in tumours and the resulting tumour growth inhibition. It also tests the concept of high-dose intermittent dosing, its impact of PK/PD modelling and limitations for clinical studies.

Methods

Cell culture
All cell lines were cultured in RPMI 1640 + 10% fetal calf serum +1% glutamine. All cells were obtained from the American Type Culture Collection.

Immunoblotting
Tumour tissue lysates were prepared as previously described (Holt *et al.*, 2012). Briefly, protein lysates were prepared from frozen tumours using the FastPrep-24 (MP Biomedicals, Solon, OH, USA) in 10 × lysis buffer (Cell Signalling Technology, Danvers, MA, USA) diluted to 1 × in PBS containing phosphatase inhibitor cocktails I and II (Sigma, St Louis, MO, USA) and protease inhibitor cocktail (Sigma). Protein concentration was determined by BCA assay (Pierce, Cramlington, UK). Immunoblots were stained with anti-total S6 (Cell signalling Technology), pS6 (Ser$^{240/244}$; Cell signalling Technology), pAkt (Ser^{473}, Cell signalling Technology), Akt (Cell signalling Technology) and glyceraldehyde-3-phosphate dehydrogenase (GAPDH, 1:2000; Abcam).

Mesoscale discovery protein analysis platform
Lysates were diluted in PBS to a final concentration of 0.5-mg·mL^{-1}, and 25 µL of lysate was added per well to the Mesoscale Discovery plates; pAktSer^{473}/total Akt duplex and pS6 Ser$^{240/244}$/total S6 duplex. Assays were carried out according to the manufacturers' guidelines.

Immunohistochemistry
Ki67 nuclear staining was carried out using formalin-fixed, paraffin-embedded xenografts tissue sections. Ki67 immunohistochemical nuclear staining was scored using an algorithm developed for scoring percentage positive nuclei on an ACIS II image analyser (ChromaVision Medical Systems, Inc.) using standard threshold settings.

In vivo efficacy studies
All animal care and experimental procedures complied with institutional guidelines and all current regulations and standards of the Home Office UK and were approved under UK Home Office Project Licence 30/2934. Animal studies are reported in compliance with the ARRIVE guidelines (Kilkenny *et al.*, 2010; McGrath & Lilley, 2015). Specific, pathogen-free, female mice (nu/nu: Alpk) were bred in house. They were housed and maintained in specific, pathogen-free conditions. The mice were used between the ages of 8 and 12 weeks in accordance with, and all procedures were carried out Human tumour xenografts were established by s.c. injection into the left-hand flank of $1-5 \times 10^{6}$ cells depending of the models in a final volume of 0.1 mL. When the mean tumour volume reached ~0.2 cm^3, the mice were randomized into vehicle ($n = 12–14$) or AZD8055-treated groups ($n = 8–12$). Tumour volumes (measured by calliper), animal body weight and tumour condition were recorded twice weekly for the duration of the study. Tumour volume was calculated as (length × width) ×

$\surd$(length × width) × ($\pi/6$) (Tomayko and Reynolds, 1989). Growth inhibition from the start of treatment was assessed by comparison of the differences in tumour volume between control and treated groups. Because the variance in mean tumour volume data increases proportionally with volume (and is therefore disproportionate between groups), data were log-transformed to remove any size dependency before statistical evaluation. Statistical significance was evaluated using a one-tailed, two-sample t-test. Mice were killed by CO_2 euthanasia.

Pharmacokinetic/pharmacodynamic studies

Animals were randomized ($n = 3$–9 per group) when tumours reached an average of 0.7 cm^3 and were humanely killed and samples collected at indicated time-points following drug administration. Tumour tissue was cut into two pieces; one half was snap frozen in liquid nitrogen and transferred to −80°C for PD analysis (using immunoblotting or mesoscale), whereas the other was fixed in 10% formalin buffer for 24 h and embedded in paraffin for immunohistochemical staining. Total blood was collected by intracardiac puncture, and plasma was prepared and immediately frozen at −20°C for PK analysis. Plasma samples were extracted by online solid phase extraction and analysed by HPLC/MS using a reversed-phase SunFire C18 RP column (Waters) and a gradient mobile phase containing water : acetonitrile : formic acid. Peaks were detected using an AB Sciex API5000. The assay had a range of 0.3–50 ng·mL^{-1}.

PK/PD modelling

All modelling was performed in ACSLX v 2.5(Aegis Technologies, 410 Jan Davis Drive, Huntsville, AL 35806). Models as described below were defined as differential equations and solved numerically. Parameter estimates were obtained using nonlinear least-squares regression: the model predictions were compared with the observed data using the sum of the square difference between the model and the data, this value being minimized by varying the model parameter values. For the PK data, it was assumed that the measurement noise was proportional to the signal to account for the several orders of magnitude displayed in the data and so residuals were weighted by the model prediction. Supporting Information-Figure S2 demonstrates the variation of the data about the model prediction is uniform on a log-scale confirming this assumption. For the PD and tumour volume data, it was assumed that measurement error was constant and so unweighted residuals were used. Again, the diagnostic plots shown in Supporting Information Figures S3, S4 and S5 show that the variation of the data around the model prediction is uniform.

The model is composed of three modules, a linear compartmental PK model, indirect response models representing the effects on pAkt Ser^{473} and pS6 Ser$^{240/244}$ and then an adaptation of the model reported by Simeoni *et al.* (2004). The model makes a number of assumptions that are then validated against the data:

1. The PK is linear.
2. Plasma concentration may be used as a surrogate for tissue exposure.
3. Inhibition of biomarker is directly correlated with tumour growth inhibition. That is, if the biomarkers are reduced

by 50% of control, then the tumour will grow at 50% of the control rate *at that point in time*.

Pharmacokinetic model

Measured plasma levels of drug after dosing in the pharmacology studies were supplemented by richly sampled low-dose oral and *intravenous* data obtained in discrete PK studies. After some model development, a linear two-compartment model with two rates of absorption for oral doses was chosen (Figure 1).

$$\frac{dGUT_{FAST}}{dt} = -ka_{FAST}GUT_{FAST}$$

$$\frac{dGUT_{SLOW}}{dt} = -ka_{SLOW}GUT_{SLOW}$$

$$\frac{dCEN}{dt} = -\frac{(Q+CL)}{V_1}CEN + \frac{Q}{V_2}PER + ka_{FAST}GUT_{FAST}$$

$$+ka_{SLOW}GUT_{SLOW}\frac{dPER}{dt} = Q\left(\frac{CEN}{V_1} - \frac{PER}{V_2}\right)$$

where predicted plasma concentration of AZD8055 is described by the following:

$$C_p = \frac{CEN}{V_1}$$

Here, *CEN* is the central compartment identified with blood, and PER is the peripheral compartment often identified with tissue. The model therefore characterizes the clearance, CL and volume of distribution, V1 + V2, when PK data
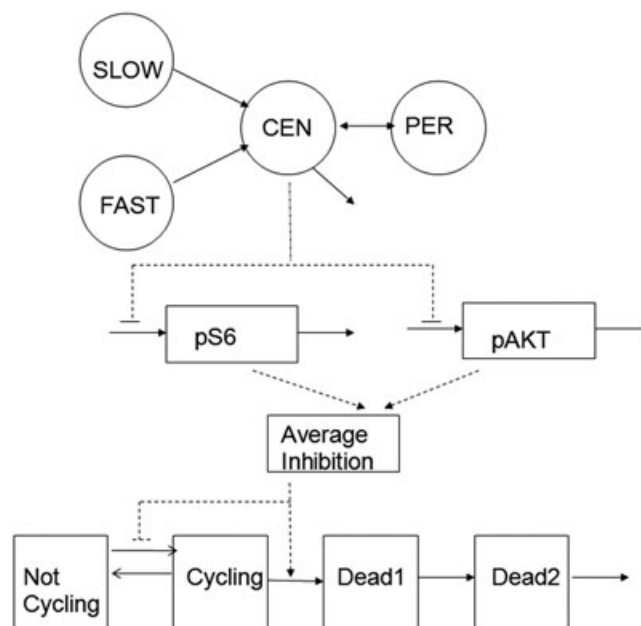
Figure 1

Diagram of the mathematical PKPD and efficacy model. The model is arranged into three distinct modules. The first is the PK model, and the second links the modelled plasma drug concentration to the effects of the drug on the biomarkers. The third module is a model of xenograft growth over time. Drug effect was linked to xenograft growth *via* the biomarkers.

from iv dosing are included in the analysis (as they are here). It also characterizes the bioavailability and rate of oral absorption in the mouse: GUT_{FAST} represents rapid absorption with rate ka_{FAST} and GUT_{SLOW} represents slower absorption with rate ka_{SLOW}. A parameter *frac* defines the fraction of the dose that is absorbed at the fast rate. The model can be calibrated against existing PK data and used to simulate PKs for experiments where PK data could not be derived.

Pharmacodynamic model

Mechanistically, inhibition of the mTOR kinase will result in a reduction in the phosphorylation of the two downstream biomarkers, pAkt Ser[473] and pS6 Ser[240/244]. This is represented mathematically by an indirect response model with inhibition of phosphorylation (Figure 1).

The model form is the same for the two biomarkers, and so, the generic form of the type I (Dayneka *et al.*, 1993) indirect response model is shown for biomarker response R

$$\frac{dR}{dt} = R_0 kout \left(1 - \frac{I_{\max}C_p}{IC50 + C_p}\right) - kout.R$$

Here, R_0 is the baseline phosphorylated level, $I_{\max}$ is the maximum level of inhibition achievable, IC_{50} is the concentration required to achieve 50% of the maximal inhibition and kout described the rate of decay of the response. In the situation considered here, kout can be considered to be the rate of de-phosphorylation.

Similar to the PK model, the PD model can be calibrated against existing data and used to simulate PD for experiments where data could not be derived.

Xenograft growth model

The study used a modified descriptive 'Simeoni' model of Xenograft, with or without drug treatment as described by Rocchetti *et al.* (2005). Tumour volume is predicted as the sum of the four states.

$$INHIB = \left(P\frac{AKT}{AKT_0} + (1-P)\frac{S6}{S6_0}\right)$$

$$MRT = \frac{1}{\lambda_0 INHIB}$$

$$\frac{dNonCycling}{dt} = 2Cycling^*(\lambda_0{}^*INHIB) - \frac{\lambda_0 NonCycling}{\left(1 + \left(\frac{\lambda_0}{\lambda_1}NonCycling\right)^\phi\right)^{\frac{1}{\phi}}}$$

$$\frac{dCycling}{dt} = \frac{\lambda_0 NonCycling}{\left(1 + \left(\frac{\lambda_0}{\lambda_1}NonCycling\right)^\phi\right)^{\frac{1}{\phi}}} - Cycling^*(\lambda_0{}^*INHIB) - Cycling\frac{E_{\max}MRT^N}{MRT^N + MRT50^N}$$

$$\frac{dDEAD_1}{dt} = Cycling\frac{E_{\max}MRT^N}{MRT^N + MRT50^N} - K_1 DEAD_1$$

$$\frac{dDEAD_2}{dt} = K_1(DEAD_1 - DEAD_2)$$

$$Volume = NonCycling + Cycling + DEAD_1 + DEAD_2$$

In the mathematical model of tumour growth, there are two compartments representing cells progressing through the cell cycle (*Cycling*) and cells in phase G0 (*NonCycling*). The rate that cells enter the cycling state becomes more limited as the tumour increases in volume, as characterized by the switching parameter ϕ and shows the same exponential to linear growth behaviour as the model from which it was adapted. To simulate cell growth, for a given cell volume

leaving the cycling compartment, twice the volume arrived in the NonCycling compartment to represent mitosis. In the model equations, λ_0 is the exponential rate of growth and λ_1 is the linear growth rate for larger tumour sizes, similar to the Simeoni model. The model was modified to test whether the antitumour effect could be predicted based on the extent and duration of the PD effects: Inhibition of growth (proliferation), *Inhib*, was a function of the relative inhibition of the two biomarkers; inhibition of cells progressing through the cell cycle was modelled by passage of cells from the Cycling to the NonCycling compartment (and the consequent cell doubling) being reduced proportional to the biomarker inhibition. Importantly, it is assumed that at 100% biomarker inhibition, the tumour stopped growing. The parameter P represented the relative importance of the two biomarkers for predicting tumour growth. Here, AKT_0 and $S6_0$ are the baseline PD parameters.

This model only predicts a cytostatic effect as a maximum. To reflect regressions seen in some cases, an additional cell death effect was added as the third term of the *Cycling* differential equation. E_{max} is the maximum rate of cell kill attainable. *MRT* is the average residence time of cells in the *Cycling* state, and *MRT50* is the value the *MRT* has to be extended to (due to reduction in proliferation) for cell death to occur in the model. The parameter N defines the steepness of this relationship between proliferation reduction and cell kill. Thus, this effect characterizes the relationship between cell cycle inhibition and cell death.

There are two additional compartments ($DEAD_1$ and $DEAD_2$) that represent cells that have been killed but still form part of the tumour mass. These compartments provided a delay between cell kill and the reduction in tumour volume, characterized by the parameter K1 (Table 1). Two delay compartments were found to be sufficient.

Data and statistical analysis

The data and statistical analysis comply with the recommendations on experimental design and analysis in pharmacology (Curtis *et al.*, 2015). For *in vivo* studies, data were log-transformed to remove any size dependency before statistical evaluation. Statistical significance was evaluated using a one-tailed, two-sample *t*-test.

Materials

AZD8055 was synthesized by AstraZeneca Inc (Alderley Park, UK). Purity was >97%. For administration by oral gavage, AZD8055 was solubilized in 30% (*w/v*) Captisol, pH 5.0. For i.p. administration, AZD8055 was dissolved in water for injection. All other chemicals were from Sigma Aldrich (St Louis, MO, USA) unless specified.

Nomenclature of targets and ligands

Key protein targets and ligands in this article are hyperlinked to corresponding entries in http://www.guidetopharmacology.org, the common portal for data from the IUPHAR/BPS Guide to PHARMACOLOGY (Southan *et al.*, 2016), and are permanently archived in the Concise Guide to PHARMACOLOGY 2015/16 (Alexander *et al.*, 2015a,b).

Table 1

Estimated PD and Efficacy model parameters (%SE in parentheses). Data shown in Figures 2, 3 and 4 were used for model calibration. Percentage biomarker inhibition required for cell death is calculated from MRT50.

| Model	Tumour type	pAkt Ser473 IC50 nM	pS6 Ser240/244 IC50 nM	Dose and schedule (mg·kg−1 qd)	TGI (%) at 20 mg·kg−1	% biomarker inhibition for cell death	Emax, maximum death rate h−1	Control growth rate h−1	KI67% positive	K1·h−1
U87MG	GBM	25 (4.5)	70 (8.7)	20	85	90 (67)	0.0842 (32)	0.0278 (13)	-	0.211 (90)
Lovo	CRC	64 (4.8)	20 (24)	20	66	-	-	0.00421 (18)	-	-
A549	NSCLC	14 (28)	1 (NWD)	20	99	95 (99)	8.06e-06 (45)	0.00728 (21)	-	0.0656(83)
Calu-6	NSCLC	1500 (NWD)	34.8 (5.6)	20	45	-	-	0.00958 (19)	-	-
Calu-3	NSCLC	82.9 (32)	80.0 (NWD)	20	125	90 (36)	0.00319 (42.8)	0.00359 (4.2)	39.4	0.03128 (72)
BT474	Breast	31.5 (19)	40.0 (47)	20	94	-	-	0.00628 (27)	34.0	-
MCF-7	Breast	72.7 (60)	34.5 (36)	20	92	95(38)	0.00679 (18)	0.0128 (13)	67.0	0.285 (110)
H460	NSCLC	88.4 (9.8)	49.3 (12)	20	62	-	-	0.0165 (18)	-	-
786-O	kidney	175(26)	1000 (31)	10	82	-	-	0.00247 (23)	18.3	-
HCT-116	CRC	422 (NWD)	3490 (NWD)	20	26	-	-	-	-	-

Results

Pharmacokinetic/pharmacodynamic/efficacy model following oral administration of AZD8055

The PK profile of AZD8055 was determined following a single administration of 1.25 to 20 mg·kg^{-1} once daily in mice bearing U87-xenografts. The linear PK model described the observed PK well (Figure 2A and Supporting Information Figure S2). The total volume of distribution was 2.94 L·kg^{-1}, and the clearance was 2.89 L·h^{-1}·kg^{-1} (Supporting Information Table S1). After an initial rapid absorption phase, there was evidence of a slow second absorption phase resulting in an oral half-life longer than that following iv administration (data not shown). Biomarkers pAkt Ser^{473} and pS6 Ser$^{240/244}$ (Figure 2B, C) measured over time in tumour xenografts using immunoblotting were also modulated in a dose-dependent manner confirming previous studies (Chresta *et al.,* 2010). The PK/PD model could describe the observed reduction in phosphorylated protein as a function of drug concentration. Interestingly, although the drug action was best described by an indirect effect, the turnover (de-phosphorylation) of the biomarkers was so rapid that it collapsed to a direct effect. There was a direct relationship between plasma PK and biomarker inhibition (Supporting Information Figure S1), and the model fitted well the observed data for both biomarkers (Supporting Information Figures S3 and S4). Previously published *in vitro* data (Chresta *et al.,* 2010) estimated IC$_{50}$ values of between 5 and 20 nM in U87-MG, A549 and MCF7 cell lines. The *in vivo* estimates are greater than this range in some cases; however, pS6 and pAkt are influenced by environmental conditions. The free fraction in mouse plasma of AZD8055 is 4% (Pike *et al.,* 2013) suggesting greater total concentrations in mouse plasma would be required to achieve free concentrations comparable with the *in vitro* values.

The mathematical model could describe the efficacy resulting from dosing AZD8055 orally in the U87-MG xenograft model (Figure 2D and Supporting Information Figure S5) without the need for the additional cell death effect. Thus, the duration and magnitude of biomarker inhibition were both important for efficacy.

Prediction of the antitumour activity across models based on pharmacodynamic profile and proliferation rate

The next step was to test whether the predictive model built for U87-MG xenografts was applicable to other tumour xenografts. AZD8055 was tested for both its PD effect and tumour growth inhibition in 10 preclinical models from five different tumour types (Table 1). All models except 786-O were tested at 20 mg·kg^{-1}. One of the early observations was that the *in vivo* IC$_{50}$ values for pAkt Ser^{473} and pS6 Ser$^{240/244}$ determined using immunoblotting across the cell lines used to generate the xenografts were not able to explain the antitumour effect observed following chronic dosing at 20 mg·kg^{-1}: for example, the A549 model showed very low IC$_{50}$ values (14 and 1 nM, for pAkt Ser^{473} and pS6 Ser$^{240/244}$, respectively) but induced a lower antitumour effect (TGI = 85%) compared with the Calu-3 model (TGI = 125%), which showed higher IC$_{50}$ values (83 and 80 nM, for pAkt Ser^{473} and pS6 Ser$^{240/244}$,
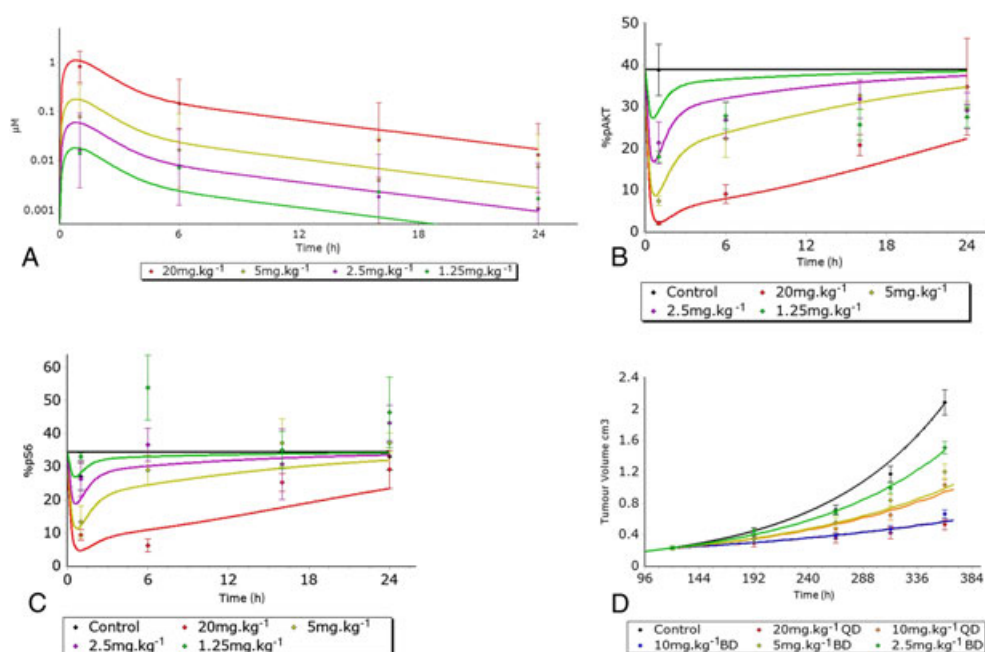
Figure 2
PK/PD and efficacy in U87MG cell line after administration of 1.25, 2.5, 5 and 20 mg·kg^{-1} AZD8055. Both experimental (dots) and modelled (lines) data are presented. (A) PK profile showing mean plasma concentration various concentrations of AZD8055 following a single oral dose; (B) pAkt Ser^{473} PD; (C) pS6 Ser$^{240/244}$ PD; (D) antitumour efficacy. All phospho levels were normalized to total protein levels and presented as a percentage of the control. The data from this study were plotted against the predicted model over time. Data shown are means ±SEM.

respectively). This disconnect between *in vivo* primary PD when continuously exposed to the compound and efficacy suggests that anti-tumour activity is driven by a second effect of cell death. This might explain the increased efficacy in some xenografted cell lines. Given that regression was observed in the Calu-3 model, the second drug effect of cell death was incorporated into the model that becomes important when the biomarker model predicts profound inhibition of the target. This was then tested against the experimental data (Figure 3). In particular, the parameter estimates (Table 1) show that a significant modelled cell death effect (E$_{max}$) is required for the Calu3 xenografts to explain the higher efficacy compared with the A549 model. The percentage of cells positive for Ki67 in control tumours correlated positively with the modelled control growth rate (Table 1), demonstrating that modelled growth rate inferred by the modelled passage of cells through the cell cycle does correspond to the measured proliferating compartment.

Overall, these data suggest that based on the overall modulation of the biomarkers over time, it is possible to predict the extent of the tumour growth inhibition in preclinical models with different sensitivity to AZD8055: reduction of proliferation predicted by biomarker reduction and a modelled cell death effect is predicted for biomarker inhibition >90%.

The antitumour efficacy of AZD8055 is only partly driven by high Cmax

Previous work from Solit *et al.* (2005) highlighted the potential benefit of high intermittent exposure to maximize the

antitumour effect. This concept is ideally suited for compounds with short half-life like AZD8055, and a recent report from Rodrik-Outmezguine *et al.* (2011) concluded that duration of biomarkers was an important determinant of efficacy, something that would not occur after intermittent dosing. In order to test the contribution of a high Cmax to the antitumour effect, AZD8055 was administered i.p. in animals bearing U87-MG xenografts to generate a PK profile with a shorter half-life than that of oral dosing. It was hypothesized that this would result in a reduced duration of biomarker modulation compared with oral dosing. A dose of 20 mg·kg^{-1} i.p. (Figure 4A) achieved a Cmax of higher than after administration of 20 mg·kg^{-1} by oral gavage. However, the clearance was more rapid after i.p. dosing resulting in reduced duration of exposure. Phospho-Akt decreased rapidly after i.p. administration to 9.5% of basal level after 30 min but recovered to baseline levels by 16 h (Figure 4B). The antitumour effect of AZD8055 in U87 xenografts was lower after administration of 20 mg·kg^{-1} AZD8055 i.p. (TGI = 65%) compared with 20 mg·kg^{-1} oral (TGI = 85%), confirming that the duration of biomarker modulation was an important component driving the antitumour effect. Indeed, the model (Figure 4C) could account for the differences in efficacy observed after oral and i.p. administration.

High-dose intermittent administration of AZD8055 alters the PK/PD/efficacy relationship

To establish whether prolonged high dose of AZD8055 was necessary to maximize the antitumour effect, AZD8055 was
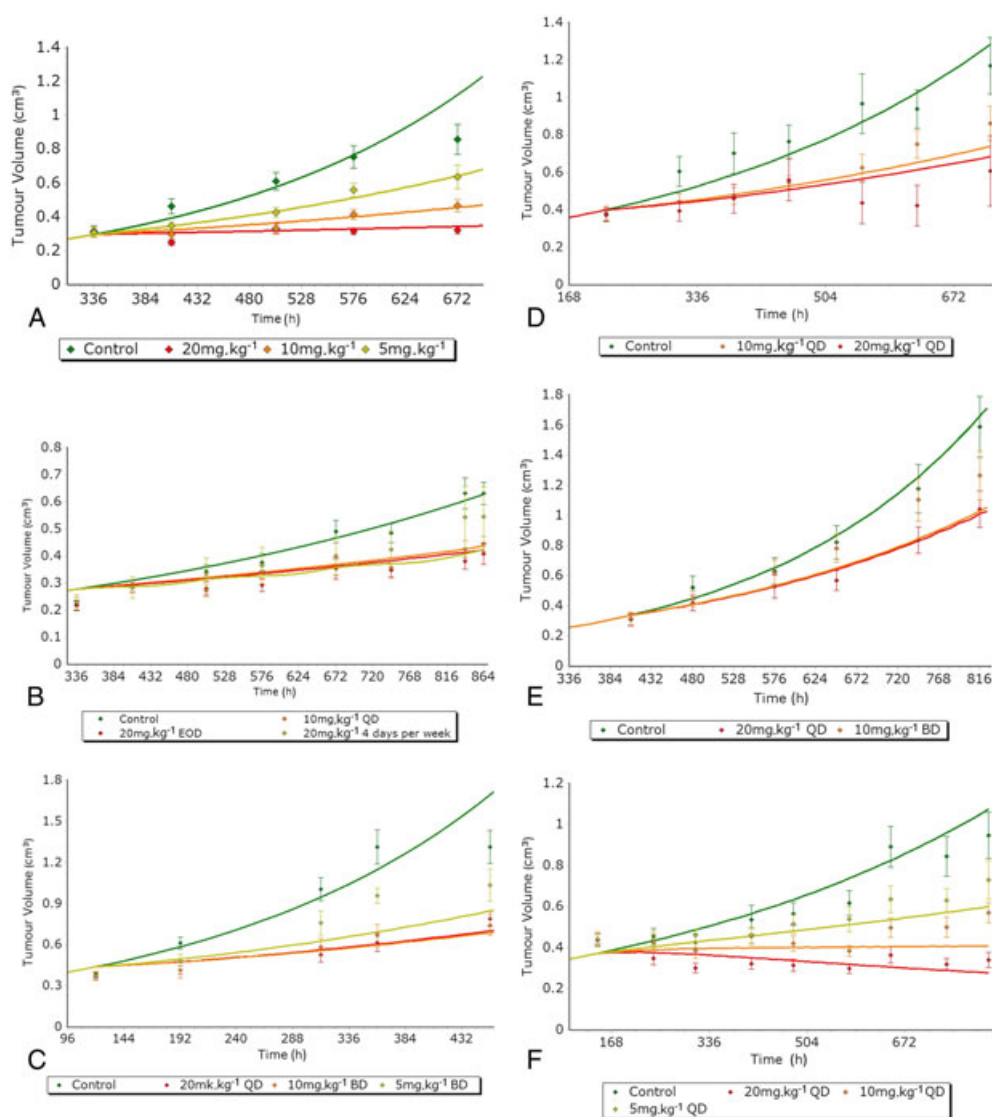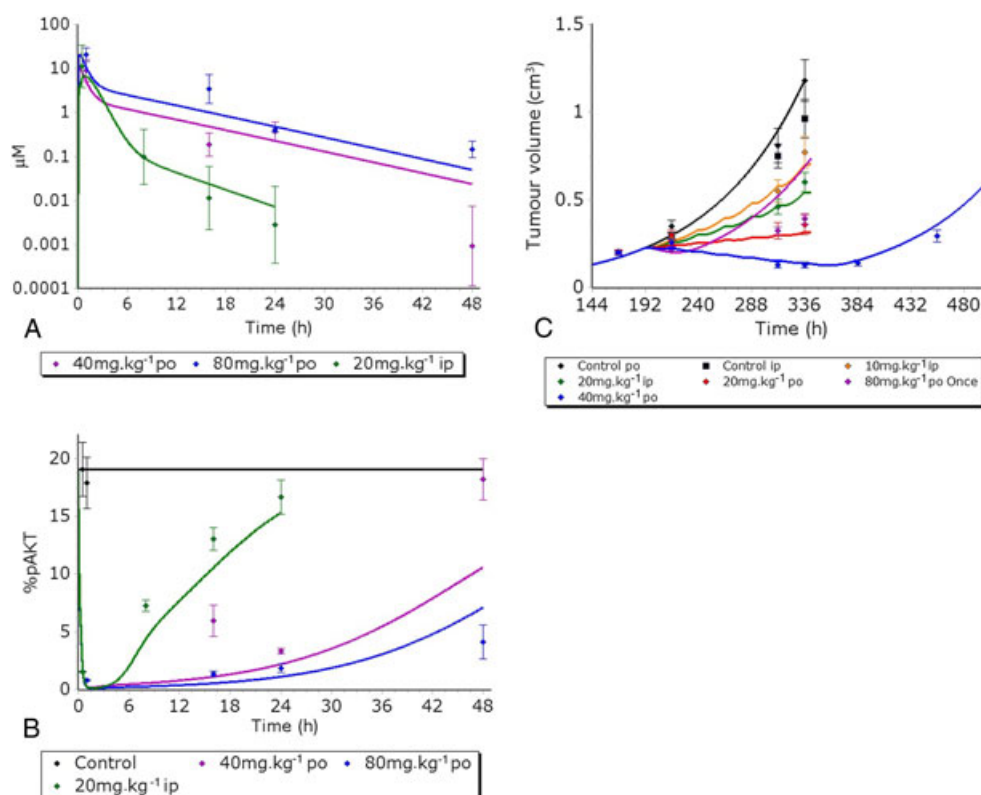
Figure 3

Antitumour efficacy predicted from the model across multiple cell line xenografts. Experimental (dots) and modelled (line) data are presented. (A) MCF-7; (B) A549; (C) LoVo; (D) BT474c; (E) CaLu-6; (F) CaLu-3.

administered by oral gavage at 40 mg·kg^{-1} once daily chronically or 80 mg·kg^{-1} once weekly. The Cmax observed after administration of 40 mg·kg^{-1} AZD8055 (9.1 µM) was similar to that observed after i.p. administration of 20 mg·kg^{-1} AZD8055. However, the PK profile was altered after oral dosing with prolonged high concentrations of AZD8055 observed up to 24 h after drug administration. This was even more apparent following administration of 80 mg·kg^{-1} AZD8055 orally with a Cmax of 20 µM and plasma concentrations greater than 1 µM observed 48 h after administration (Figure 4A).

This change in PK profile was associated with a profound change in biomarker profile (Figure 4B): pAkt Ser[473] (determined by Mesoscale) was reduced to 5.9% of basal level within an hour after drug administration (both 40 and 80-mg·kg^{-1} AZD8055). The recovery was much slower than after i.p. administration with a progressive recovery of pAkt Ser[473]

levels was observed over 48 h, consistent with the progressive decay in drug concentrations in plasma and the previously developed PK/PD model. The oral administration of 40 mg·kg^{-1} AZD8055 once daily induced a rapid reduction in tumour volume (Figure 4C), and this antitumour effect was maintained for the duration of treatment (TGI = 107%). The administration of AZD8055 at a dose of 80 mg·kg^{-1} once weekly resulted in a superior anti-tumour activity compared with the i.p. and low oral doses, with regression being apparent early after the start of the treatment. However, tumour growth resumed during the drug holiday. Interestingly, overall, the 20 mg·kg^{-1} p.o. daily schedule resulted in comparable tumour growth inhibition to that of the 80 mg·kg^{-1} once weekly.

The modelling would suggest that the profound and prolonged pathway inhibition induces sufficient cell death that the tumour cannot recover in the washout period. Prolonged inhibition of proliferation would also be an

Figure 4
PK/PD and efficacy following high intermittent oral dosing and i.p. administration. (A) PK of AZD8055; (B) PD effects of AZD8055; (C) Antitumour effect of AZD8055.

important factor. These observations are accounted for in the model (Figure 4C), with both i.p. and high-dose oral treatment inducing cell death initially, but only the continued oral dose maintaining anti-tumour effect through the modelled anti-proliferation. This suggests that a once weekly high-dose administration of the compound has comparable benefit with a continuous dosing schedule at a lower concentration. However, the exposure to the compound are high concentrations maintained for 48 h, with the flat PK profile looking similar to that achieved with a continuous infusion (Figure 4A). All PD and tumour model parameters are reported in Supporting Information Table S2.

Discussion

The current PK/PD/efficacy model links for the first time temporal biomarker modulation and reduction in tumour growth across a range of preclinical models with different sensitivity to the mTOR kinase inhibitor AZD8055. The model retains its predictive power when different routes and schedules of administration of AZD8055 are used.

PK/PD/efficacy models are highly dependent on the preclinical models used to build them. Engineered preclinical models or very sensitive models may overestimate the antitumour effect achievable in the clinic and may not be representative of the patient population treated with the agent. In this study, a PTEN-negative U87-MG glioblastoma

xenograft was used to build the PK/PD/efficacy model. Mutations in PTEN are observed in ~ 30% of glioblastoma tumours (Brennan *et al.*, 2013). PTEN loss has been shown to activate the PI3K pathway and to be associated with shorter survival in patients with glioblastoma (Yao *et al.*, 2012). However, in spite of the potential relevance of the U87-MG xenograft model, it has an extremely rapid growth rate and may be an outlier, so additional non-engineered xenograft models were also used to validate the initial PK/PD/efficacy model. The PK/PD/efficacy model described with the PI3K inhibitor GDC-0980 by Salphati *et al.* (2012) used an engineered xenograft model overexpressing human Her2 in an oestrogen-dependent breast cancer model MCF7. The predicted human daily dose to be associated with significant antitumour effect in the engineered model was 55 mg GDC-0980. Phase 1 study reported antitumour activity in three patients with mesothelioma at doses lower than 50 mg (Wagner *et al.*, 2011), so it is possible that a PK/PD/efficacy model built with mesothelioma xenografts may have predicted a different efficacious dose than the engineered model.

PK/PD/efficacy models are often based on an exponential growth of the tumour xenografts, which may be accurate for fast growing xenograft models but may not reflect slow growing tumours in patients. In this study, a modified descriptive model of tumour growth rate as described by Simeoni *et al.* (2004) was used, and a relationship between Ki67 and growth rate estimated by the model was confirmed in control animals (Table 1). Ki67 has been used as an early indicator of tumour

response to the mTOR inhibitor everolimus in breast cancer using paired tumour biopsies pre-and post-treatment (Baselga *et al.*, 2009), so it may be possible to incorporate this biomarker in a predictive model of response in patients.

The mathematical modelling developed in the current study links biomarker modulation and reduction in tumour growth over time. This contrasts with previous PK/PD/efficacy studies linking a target concentration or biomarker threshold to be maintained chronically in order to drive antitumour efficacy. For example, Kogame *et al.* (2013) established a PK/PD/efficacy model for the **Smo** inhibitor **TAK-441** in the PAN-04 xenograft model using biomarker assessment in tumour and skin and concluded that >83% reduction in Gli1 mRNA in the tumour was required for tumour stasis. Similarly, tumour stasis was achieved with the PI3K inhibitor GDC-0941 in MCF7.1 xenografts when plasma concentrations of ~0.3 uM were maintained continuously (Salphati *et al.,* 2010). This type of approach is limited when intermittent dosing is proposed, so the current study evaluated the ability of the PK/PD/efficacy model to predict antitumour efficacy when altering different routes or schedules of administration. Delivering high concentrations of AZD8055 for a short duration, by i.p. dosing, did modulate the biomarkers transiently and did not produce a significant antitumour effect while prolonged high concentrations of AZD8055 maximizing biomarker modulation over time delivered the best antitumour effect. This supported the hypothesis that overall modulation of biomarkers over time was the main driver for efficacy. It also supported the concept first developed by Solit *et al.* (2005) with gefitinib that profound inhibition of a signalling pathway can switch the biological effect from growth inhibition to cell death by abolishing feedback loops. Importantly, the PK/PD/efficacy model still robustly predicted the antitumour effect observed even with an intermittent dosing schedule. A preclinical PK-efficacy model using the mTOR inhibitor **MLN0128** used a tumour xenograft in conjunction with the clinical PK parameters to simulate tumour volume-time curves for various MLN0128 doses/schedules was recently reported (Patel *et al.,* 2013). It will be interesting to see whether additional parameters related to adverse events can be embedded in the future models, especially if intermittent dosing is driven by the mitigation of adverse events. The work reported here supports the possibility of two alternative schedules for dual mTOR inhibitors: continuous dosing to ensure continuous target coverage or an alternative high-dose intermittent schedule that would have to achieve complete target inhibition, at least around PK Cmax, to be as effective. Such regimens have been investigated for the dual mTOR kinase inhibitor **AZD2014**.

Overall, the findings from this study and the previously cited works indicate the potential predictive value of pharmacodynamically led efficacy analysis that could result in the reduction of the number of xenograft experiments required to guide dosing of previously untested compounds in efficacy studies.

Acknowledgements

Author contributions

S.M.G, J.W.T.Y., S.V.H., A.L., B.D. and R.W.W. participated in research design. A.L., S.V.H., K.P. and K.W. conducted experiments. J.W.T.Y., S.V.H. and S.M.G. performed data analysis. J.W.T.Y., S.M.G. and B.R.D. wrote or contributed to the writing of the manuscript.

Conflict of interest

All authors are employees of AstraZeneca or MedImmune.

Declaration of transparency and scientific rigour

This Declaration acknowledges that this paper adheres to the principles for transparent reporting and scientific rigour of preclinical research recommended by funding agencies, publishers and other organisations engaged with supporting research.

References

Alexander SPH, Fabbro D, Kelly E, Marrion N, Peters JA, Benson HE *et al.* (2015a). The Concise Guide to PHARMACOLOGY 2015/16: Enzymes. Br J Pharmacol 172: 6024–6109.

Alexander SPH, Davenport AP, Kelly E, Marrion N, Peters JA, Benson HE *et al.* (2015b). The Concise Guide to PHARMACOLOGY 2015/16: G protein-coupled receptors. Br J Pharmacol 172: 5744–5869.

Baselga J, Semiglazov V, van DP, Manikhas A, Bellet M, Mayordomo R *et al.* (2009). Phase II randomized study of neoadjuvant everolimus plus letrozole compared with placebo plus letrozole in patients with estrogen receptor-positive breast cancer. J Clin Oncol 27: 2630–2637.

Brennan CW, Verhaak RG, McKenna A, Campos B, Noushmehr H, Salama SR *et al.* (2013). The somatic genomic landscape of glioblastoma. Cell 155: 462–477.

Chiarini F, Evangelisti C, McCubrey JA, Martelli AM (2015). Current treatment strategies for inhibiting mTOR in cancer. Trends Pharmacol Sci 36: 124–135.

Chresta CM, Davies BR, Hickson I, Harding T, Cosulich S, Critchlow SE *et al.* (2010). AZD8055 is a potent, selective, and orally bioavailable ATP-competitive mammalian target of rapamycin kinase inhibitor with in vitro and in vivo antitumor activity. Cancer Res 70: 288–298.

Cloughesy TF, Yoshimoto K, Nghiemphu P, Brown K, Dang J, Zhu S *et al.* (2008). Antitumor activity of rapamycin in a Phase I trial for patients with recurrent PTEN-deficient glioblastoma. PLoS Med 5: e8.

Curtis MJ, Bond RA, Spina D, Ahluwalia A, Alexander SP, Giembycz MA *et al.* (2015). Experimental design and analysis and their reporting: new guidance for publication in BJP. Br J Pharmacol 172: 3461–3471.

Dayneka NL, Garg V, Jusko WJ (1993). Comparison of four basic models of indirect pharmacodynamic responses. J Pharmacokinet Biopharm 21: 457–478.

Garcia-Martinez JM, Alessi DR (2008). mTOR complex 2 (mTORC2) controls hydrophobic motif phosphorylation and activation of

serum- and glucocorticoid-induced protein kinase 1 (SGK1). Biochem J 416: 375–385.

Holt SV, Logie A, Davies BR, Alferez D, Runswick S, Fenton S *et al.* (2012). Enhanced apoptosis and tumor growth suppression elicited by combination of MEK (selumetinib) and mTOR kinase inhibitors (AZD8055). Cancer Res 72: 1804–1813.

Kilkenny C, Browne W, Cuthill IC, Emerson M, Altman DG (2010). Animal research: reporting in vivo experiments: the ARRIVE guidelines. Br J Pharmacol 160: 1577–1579.

Kogame A, Tagawa Y, Shibata S, Tojo H, Miyamoto M, Tohyama K *et al.* (2013). Pharmacokinetic and pharmacodynamic modeling of hedgehog inhibitor TAK-441 for the inhibition of Gli1 messenger RNA expression and antitumor efficacy in xenografted tumor model mice. Drug Metab Dispos 41: 727–734.

Laplante M, Sabatini DM (2012). mTOR signaling in growth control and disease. Cell 149: 274–293.

McGrath JC, Lilley E (2015). Implementing guidelines on reporting research using animals (ARRIVE etc.): new requirements for publication in BJP. Br J Pharmacol 172: 3189–3193.

O'Reilly KE, Rojo F, She QB, Solit D, Mills GB, Smith D *et al.* (2006). mTOR inhibition induces upstream receptor tyrosine kinase signaling and activates. Akt Cancer Res 66: 1500–1508.

Patel CG, Patel M, Chakravarty E, Gangolli EA, Barry E, Westin EH *et al* (2013). Clinical pharmacokinetics (PK) and translational PK-pharmacodynamic (PD) modeling and simulation to predict antitumor response of various dosing schedules to guide the selection of a recommended phase II dose (RP2D) and schedule for the investigational agent MLN0128. *ASCO.*

Pike KG, Malagu K, Hummersone MG, Menear KA, Duggan HM, Gomez S *et al.* (2013). Optimization of potent and selective dual mTORC1 and mTORC2 inhibitors: the discovery of AZD8055 and AZD2014. Bioorg Med Chem Lett 23: 1212–1216.

Rocchetti M, Poggesi I, Germani M, Fiorentini F, Pellizzoni C, Zugnoni P *et al.* (2005). A pharmacokinetic-pharmacodynamic model for predicting tumour growth inhibition in mice: a useful tool in oncology drug development. Basic Clin Pharmacol Toxicol 96: 265–268.

Rodrik-Outmezguine VS, Chandarlapaty S, Pagano NC, Poulikakos PI, Scaltriti M, Moskatel E *et al.* (2011). mTOR kinase inhibition causes feedback-dependent biphasic regulation of AKT signaling. Cancer Discov 1: 248–259.

Salphati L, Wong H, Belvin M, Bradford D, Edgar KA, Prior WW *et al.* (2010). Pharmacokinetic-pharmacodynamic modeling of tumor growth inhibition and biomarker modulation by the novel phosphatidylinositol 3-kinase inhibitor GDC-0941. Drug Metab Dispos 38: 1436–1442.

Salphati L, Pang J, Plise EG, Lee LB, Olivero AG, Prior WW *et al.* (2012). Preclinical assessment of the absorption and disposition of the phosphatidylinositol 3-kinase/mammalian target of rapamycin inhibitor GDC-0980 and prediction of its pharmacokinetics and efficacy in human. Drug Metab Dispos 40: 1785–1796.

Simeoni M, Magni P, Cammia C, De NG, Croci V, Pesenti E *et al.* (2004). Predictive pharmacokinetic-pharmacodynamic modeling of tumor growth kinetics in xenograft models after administration of anticancer agents. Cancer Res 64: 1094–1101.

Solit DB, She Y, Lobo J, Kris MG, Scher HI, Rosen N *et al.* (2005). Pulsatile administration of the epidermal growth factor receptor inhibitor gefitinib is significantly more effective than continuous dosing for sensitizing tumors to paclitaxel. Clin Cancer Res 11: 1983–1989.

Southan C, Sharman JL, Benson HE, Faccenda E, Pawson AJ, Alexander SP *et al.* (2016). The IUPHAR/BPS guide to PHARMACOLOGY in 2016: towards curated quantitative interactions between 1300 protein targets and 6000 ligands. Nucl Acids Res 44: D1054–D1068.

Tanaka C, O'Reilly T, Kovarik JM, Shand N, Hazell K, Judson I *et al.* (2008). Identifying optimal biologic doses of everolimus (RAD001) in patients with cancer based on the modeling of preclinical and clinical pharmacokinetic and pharmacodynamic data. J Clin Oncol 26: 1596–1602.

Tomayko MM, Reynolds CP (1989). Determination of subcutaneous tumor size in athymic (nude) mice. Cancer Chemother Pharmacol 24: 148–154.

Wagner AJ, Bendell JC, Dolly S., Morgan JA, Ware JA, Fredrickson J *et al.* 6032 (2011). A first-in-human phase I study to evaluate GDC-0980, an oral PI3K/mTOR inhibitor, administered QD in patients with advanced solid tumors. *ASCO.*

Yao J, Zhao Q, Yuan Y, Zhang L, Liu X, Yung WK *et al.* (2012). Identification of common prognostic gene expression signatures with biological meanings from microarray gene expression datasets. PLoS One 7: e45894.

Supporting Information

Additional Supporting Information may be found online in the supporting information tab for this article.

https://doi.org/10.1111/bph.13886

Figure S1 Plots exemplifying the direct relationships between drug concentration in plasma and phospho- biomarker reduction. a) pAkt IC_{50} = 23 nM b)S6 IC_{50} = 70 nM.

Figure S2 Plot of observed *vs* model simulated values for pharmacokinetics.

Figure S3 Plot of observed *vs* model simulated values for pAkt.

Figure S4 Plot of observed *vs* model simulated values for pS6.

Figure S5 Plot of observed *vs* model simulated values for tumour volume.

Table S1 Pharmacokinetic parameters for AZD8055 following oral administration in mice bearing U87-MG xenoigrafts.

Table S2 PD-Efficacy model parameter estimates. Imax = 1 in all cases.